Ion implanted Si:P double-dot with gate tuneable interdot coupling

V.C. Chan,[*] T.M. Buehler,[†] A.J. Ferguson, D.R.

McCamey, D.J. Reilly,[‡] A.S. Dzurak, and R.G. Clark

Centre for Quantum Computer Technology,

Schools of Physics and Electrical Engineering & Telecommunications,

The University of New South Wales,

NSW 2052, Sydney Australia

C. Yang and D.N. Jamieson

Centre for Quantum Computer Technology,

School of Physics, University of Melbourne,

VIC 3010, Australia

(Dated: February 4, 2008)

Abstract

We report on millikelvin charge sensing measurements of a silicon double-dot system fabricated by phosphorus ion implantation. An aluminum single-electron transistor (SET) is capacitively coupled to each of the implanted dots enabling the charging behavior of the double-dot system to be studied independently of current transport. Using an electrostatic gate, the interdot coupling can be tuned from weak to strong coupling. In the weak interdot coupling regime, the system exhibits well-defined double-dot charging behavior. By contrast, in the strong interdot coupling regime, the system behaves as a single-dot.

Double-dot systems hold significant interest for both classical[1] and quantum information processing[2]. For quantum information processing (QIP), semiconductor quantum double-dots with discrete states have proven to be an excellent platform for research into quantum states and their interactions[3,4]. In the use of classical double-dots which have a continuous density of states, applications have been demonstrated in single-electron logic[5] and quantum cellular automata[6,7] (QCA). A key aspect of both classical and quantum double-dot systems is the interdot coupling, which determines the strength of the interaction between the two dots[8]. We present a double-dot system, implemented in silicon, with electrically tuneable interdot coupling. Compatibility with silicon CMOS techniques is an advantage for application in classical electronic circuits. In addition, silicon is an attractive material for realizing a spin-based quantum computer architecture for QIP[9] due to the long spin coherence times associated with phosphorus doped silicon[10].

The silicon double-dot device presented here comprises two Si:P dots and leads, with a metallic density of states, that are formed by low energy (14 keV) phosphorus ion implantation. Ion implantation provides a controllable method for creating well-defined locally doped regions in silicon capable of exhibiting single-electron charging[11]. The tunnel junctions are formed by the undoped silicon regions and have the form of nanoscale MOSFETs[12], and a surface gate provides control of the interdot coupling (Fig. 1(a)). Aluminum single-electron transistor (SET) charge sensors coupled to the Si:P dots provide a means of non-invasively detecting the charge state of the system. Charge sensing is particularly relevant for device regimes not accessible with direct transport measurements, for example for weakly coupled and few-electron quantum dots[13,14].

The device investigated was fabricated on high resistivity (> 5 kΩ.cm) n-type silicon with a thermally grown 5nm gate oxide. A 150 nm thick polymethylmethacrylate (PMMA) resist patterned by e-beam lithography was used as a mask for ion implantation. The dimensions of the dots were designed to be 70 nm $\times$ 500 nm and the device was fabricated with tunnel junction widths $w_j \simeq 100$ nm (Fig. 1(a)). Phosphorus ions at 14 keV were implanted with an areal dose of approximately 1.22×10^{14} cm^{-2} and a mean implantation depth of $\sim$20 nm. A rapid thermal anneal (RTA) was performed to repair implantation damage and electrically activate the phosphorus dopants. Surface control gates were fabricated by e-beam lithography in PMMA resist and TiAu metallisation. The aluminum SETs were fabricated by double angle evaporation with an *in situ* oxidation using a shadow mask formed in bilayer e-beam resist.

Figure 1(b) shows an SEM image of a device similar to that measured. SET_L and SET_R serve as charge sensors for the charge states of DOT_L and DOT_R, respectively. Surface gates L and R control the electrostatic potential of DOT_L and DOT_R. Gate M is positioned over the tunnel junction between the two dots and is used to control the interdot coupling. Gates G_L and G_R are

used to position the SETs to operating points of high charge sensitivity.

Electrical measurements were carried out at $T = 50$ mK in a dilution refrigerator. No magnetic field was applied to the device ($B = 0$ T) and the SETs were operated in the superconducting regime with a dc source-drain voltage applied to bias the SETs to points of high charge sensitivity. All measurements were performed in the linear transport regime of the double-dot system[8], i.e. double-dot $V_{SD} = 0$ mV. SET conductances were measured simultaneously using separate lock-in amplifiers, with an excitation voltage of 20 μV at frequencies < 200 Hz.

Figures 2(a) and (b) show SET_L and SET_R differential conductances measured as a function of V_L and V_R, with $V_M = 0$ V. The charge stability diagram of a double-dot system is given by hexagon shaped cells as a function of gate voltage V_L and V_R, each of which represent a particular charge configuration[8]. The charge occupancies of DOT_L and DOT_R are given by m and n, respectively. The horizontal (vertical) lines in the charge stability diagrams represent $LEAD_{L(R)}$ $\leftrightarrow DOT_{L(R)}$ transitions, where the charge occupancy of $DOT_{L(R)}$ is changed by one electron for adjacent hexagons, e.g. $(m, n) \rightarrow (m+1, n)$. Triple points occur when three different charge configurations are degenerate, and interdot charge transitions ($DOT_L \leftrightarrow DOT_R$) take place across the intersections of nearest neighbor triple points, e.g. $(m+1, n) \rightarrow (m, n+1)$. The direct capacitances of gates L and R to their respective dots were determined from the period of the $LEAD_{L(R)}$ $\leftrightarrow DOT_{L(R)}$ charge state transitions to be $C_{L,DOTL} \simeq 100$ aF and $C_{R,DOTR} \simeq 80$ aF, while the cross-capacitances were found to be negligible. The difference in the direct capacitance values arise from a slight misalignment between the gate and dots.

Single traces were taken from the data in Fig. 2(a), and SET_L differential conductance plotted as a function of gate L (Fig. 2(c)) and gate R (Fig. 2(d)). The 'sawtooth' behavior in Figs. 2(c) and (d) is a signature of charge state transitions as measured by charge sensing. There is a steady polarization as a function of gate voltage and then a discontinuity which signifies the detection of an electron tunnelling event. Note that the sawtooth signal arising from charge transitions in DOT_L has a larger amplitude than the signal arising from charge transitions in DOT_R. Although each SET is primarily coupled to one of the dots, a cross-capacitance between the SETs and their opposite dots results in small induced charge on the SET islands. The charge induced on the SET islands for each of the different charge state transitions was evaluated and the values are shown in Table I. The magnitude of the charge induced on the SET islands differs for each charge transition due to the different capacitances associated with each of the tunnel barriers in the device.

For interdot charge state transitions, the total charge of the double-dot system remains fixed, i.e. $(m + 1, n) \leftrightarrow (m, n + 1)$. Figure 3(a) shows a plot of SET_L differential conductance which has been differentiated with respect to V_R, enabling the triple points can be resolved more clearly

compared with Fig. 2(a). Taking a slice through the charging diagram as indicated by the diagonal line, Fig. 3(b) shows the differential conductance of SET_L corresponding to an interdot transition $(m + 1, n) \rightarrow (m, n + 1)$. The interdot transition has the form of a Coulomb 'step', and the width of the step is dependent on the interdot coupling. The interdot coupling between the two dots is characterized by the mutual capacitance[8] (C_m) and the tunnel coupling, given by the tunnel conductance[15] (G_{int}). Conductance measurements of single tunnel junctions (MOSFETs) indicate that at $V_M = 0$ V the double-dot is in the weak tunnel coupling regime ($G_{int} \ll 2e^2/h$), so C_m was treated as the dominant parameter determining the interdot coupling. The electrostatic coupling C_m was extracted from the triple point separation for a range of values of V_M.

The ratio of mutual capacitance C_m to total dot capacitance $C_{\Sigma L(R)}$ was determined from the distance between neighboring triple points by the equation $C_m/C_{\Sigma L(R)} = \triangle V^m_{R(L)}(C_{R(L)}/e)$, where $\triangle V^m_{R(L)}$ is the triple point separation in $V_R(V_L)$ space[8] (Fig. 3(a)). From Fig. 3 (a), the ratios were evaluated to be $C_m/C_{\Sigma L} \sim 0.221$ and $C_m/C_{\Sigma R} \sim 0.217$ when $V_M = 0$ V. The individual dot charging energies were not determined for the device by a finite bias measurement, however, the interdot coupling ratios indicate nearly identical charging energies for both dots which is expected from the device geometry. Figure 3(c) show SET_L differential conductance, as a function of V_L and V_R, where $V_M = + 0.81$ V. Increasing the positive voltage applied to gate M increases the interdot coupling, which is resolved as an increase in the separation between the triple points. For $V_M = + 0.81$ V, the interdot coupling ratios were evaluated to be $C_m/C_{\Sigma L} \sim 0.385$ and $C_m/C_{\Sigma R} \sim 0.416$.

As V_M is further increased, the interdot coupling increases such that $C_m/C_{\Sigma L(R)} \rightarrow 1$ (Fig. 3(d), $V_M = + 1.0$ V). The device no longer exhibits the hexagon cells of a double-dot charge stability diagram, but rather a series of parallel lines associated with single-dot charging. Each line corresponds to a transition in the charge occupancy of the 'single-dot' where the total charge is given by $m + n$. Figure 3(e) shows the interdot coupling ratios $C_m/C_{\Sigma L(R)}$ as a function of V_M. Conductance measurements of single tunnel junctions (MOSFETs) indicate that the tunnel junction between DOT_L and DOT_R remains in the weakly tunnel coupled regime, i.e. $G_{int} \ll 2e^2/h$, when $V_M = + 1.0$ V. This suggests that the increasing interdot coupling is dominated by an increase in the mutual capacitance C_m rather than an increase in the tunnel coupling G_{int}[16]. An explanation for this is the formation of an electron accumulation layer between the dots as greater positive voltage is applied to gate M, modifying the electrostatic coupling between the dots.

We have presented a Si:P double-dot system, fabricated by ion implantation, with gate tuneable interdot coupling. The implementation of a double-dot system in silicon will enable relatively straightforward incorporation into more complex circuits. Future work on the silicon double-dots presented here, will examine application in quantum cellular automata. Additionally, a significant

reduction in the size dots may allow individual quantum states to be investigated. The realization of a quantum double-dot may provide a pathway to coherent measurements of spin states in silicon, as has been demonstrated in AlGaAs/GaAs heterostructures[17].

---

* Electronic address: victor.chan@student.unsw.edu.au

† Now at ABB Switzerland, Corporate Research.

‡ Now at Dept. Physics, Harvard University

[1] C. S. Lent, P. D. Tougaw, W. Porod, and G. H. Bernstein, Nanotechnology **4**, 49 (1993).

[2] D. Loss and D. P. DiVincenzo, Phys. Rev. A **57**, 120 (1998).

[3] T. Hayashi, T. Fujisawa, H. D. Cheong, Y. H. Jeong, and Y. Hirayama, Phys. Rev. Lett. **91**, 226804 (2003).

[4] J. Gorman, D. G. Hasko, and D. A. Williams, Phys. Rev. Lett. **95**, 090502 (2005).

[5] I. H. Chan, P. Fallahi, R. M. Westervelt, K. D. Maranowski, and A. C. Gossard, Physica E **17**, 584 (2003).

[6] A. O. Orlov, I. Amlani, G. H. Bernstein, C. S. Lent, and G. L. Snider, Science **277**, 928 (1997).

[7] I. Amlani, A. O. Orlov, G. Toth, G. H. Bernstein, C. S. Lent, and G. L. Snider, Science **284**, 289 (1999).

[8] W. G. van der Wiel, S. D. Franceschi, J. M. Elzerman, T. Fujisawa, S. Tarucha, and L. P. Kouwenhoven, Rev. Mod. Phys. **75**, 1 (2003).

[9] B. E. Kane, Nature **393**, 133 (1998).

[10] A. M. Tyryshkin, S. A. Lyon, A. V. Astashkin, and A. M. Raitsimring, Phys. Rev. B **68**, 193207 (2003).

[11] V. C. Chan, D. R. McCamey, T. M. Buehler, A. J. Ferguson, D. J. Reilly, A. S. Dzurak, R. G. Clark, and C. Y. D. N. Jamieson, arXiv:cond-mat/0510373 (2005).

[12] M. Sanquer, M. Specht, and L. Ghenim, Phys. Rev. B **61**, 7249 (2000).

[13] L. DiCarlo, H. J. Lynch, A. C. Johnson, L. I. Childress, K. Crockett, C. M. Marcus, M. P. Hanson, and A. C. Gossard, Phys. Rev. Lett. **92**, 226801 (2004).

[14] J. M. Elzerman, R. Hanson, L. H. W. van Beveren, B. Witkamp, L. M. K. Vandersypen, and L. P. Kouwenhoven, Nature **430**, 431 (2004).

[15] F. R. Waugh, M. J. Berry, C. H. Crouch, C. Livermore, D. J. Mar, and R. M. Westervelt, Phys. Rev. B **53**, 1413 (1996).

[16] C. Livermore, C. H. Crouch, R. M. Westervelt, K. L. Campman, and A. C. Gossard, Science **274**, 1332 (1996).

[17] J. R. Petta, A. C. Johnson, J. M. Taylor, E. A. Laird, A. Yacoby, M. D. Lukin, C. M. Marcus, M. P. Hanson, and A. C. Gossard, Science **309**, 2180 (2005).

Transition	$\triangle q_{SETL}$ / e	$\triangle q_{SETR}$ / e
$DOT_L \leftrightarrow LEAD_L$	~ 0.074	~ 0.043
$DOT_R \leftrightarrow LEAD_R$	~ 0.042	~ 0.074
$DOT_L \leftrightarrow DOT_R$	~ 0.060	~ 0.062

TABLE I: Charge induced on $SET_{L(R)}$ for various charge state transitions in the double-dot system.

FIG. 1: (a) Cross-section schematic of the device showing the phosphorus implanted area, surface gates and SETs. (b) SEM of the device, with implanted double-dot and leads, control gates and SETs. The red shaded areas indicate regions of phosphorus ion implantation.

FIG. 2: (a) and (b) Simultaneously measured conductances signals (with a best-fit plane subtracted for clarity) from SET_L and SET_R respectively as a function of V_L and V_R ($V_M = 0$ V). A double-dot charge stability diagram is clearly resolved. Single traces are taken from (a) and SET_L conductance is plotted as a function of gate L (c) and gate R (d). The charge occupancies of DOT_L and DOT_R are given by m and n, respectively. SET $V_{ac} = 20$ μV, $T = 50$ mK and $B = 0$ T.

FIG. 3: (a) SET_L transconductance as a function of V_L and V_R ($V_M = 0$ V). The diagonal line follows an interdot charge state transition. (b) SET_L conductance (background line subtracted) as V_L and V_R are varied along an interdot transition $(m + 1, n) \leftrightarrow (m, n + 1)$. SET_L conductance as a function of V_L and V_R when (c) $V_M = + 0.81$ V, and (d) $V_M = + 1.0$ V. (e) Interdot coupling ratios $C_m/C_{\Sigma L(R)}$ as a function of V_M. SET $V_{ac} = 20$ μV, $T = 50$ mK and $B = 0$ T.
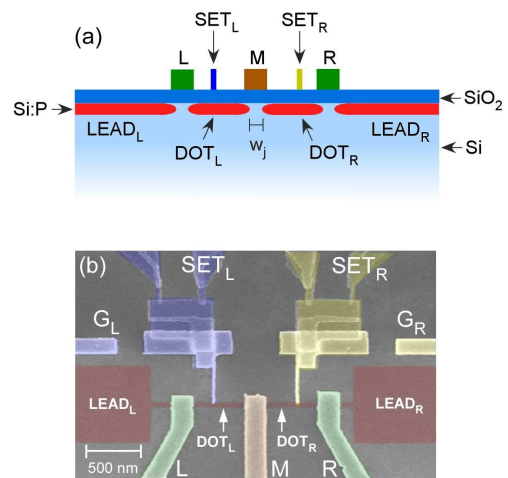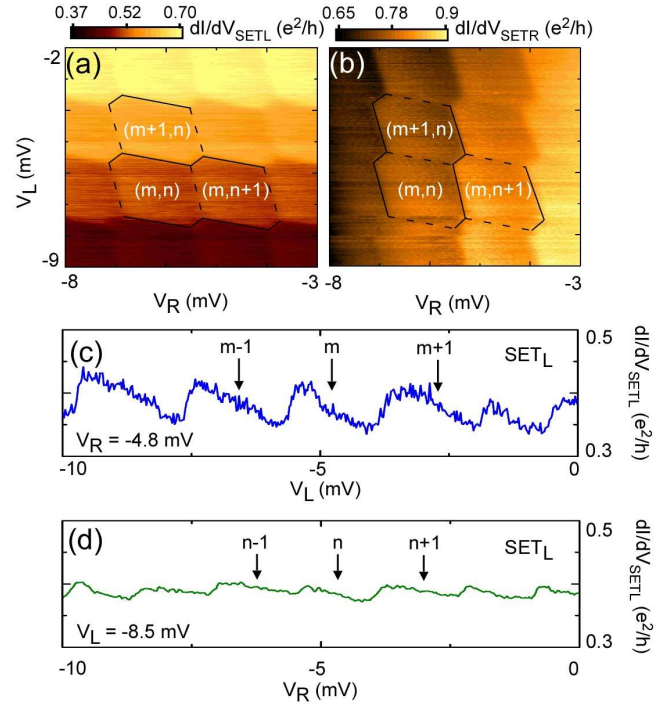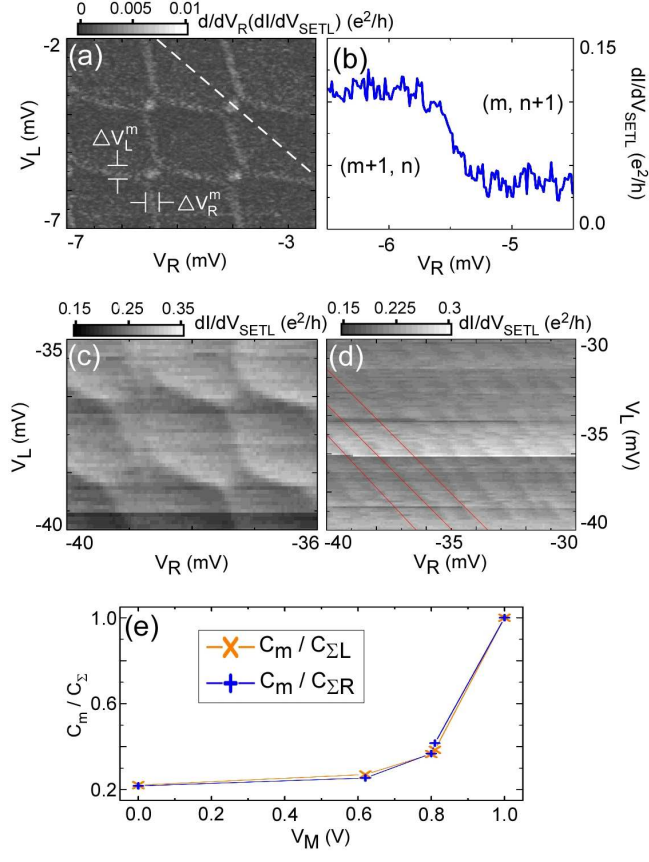
FIG. 1:

FIG. 2:

FIG. 3: